ORIGINAL PAPER

Facile synthesis of aqueous silver nanoparticles and silver/molybdenum disulfide nanocomposites and investigation of their nonlinear optical properties

Xiao-Yan Zhang[1] · Hong-Qiang Wang[2,3] · Yi Sun[4] · Wei Zhou[1] · Jun Wang[2,3,5]

Abstract

Silver nanoparticle (AgNP) aqueous colloids with different surface plasmon resonance (SPR) frequencies were controllably synthesized by a facile and green chemical synthesis method. The obtained AgNPs with an average diameter of ~ 15 nm show a symmetrical SPR peak at ~ 400 nm. Another longitudinal SPR mode at ~ 520 nm occurs when increasing the amount of ethanol according to the ultraviolet–visible light spectra. The third-order nonlinear optical (NLO) absorption properties of the AgNP colloids were found to switch from two-photon absorption (TPA) to saturable absorption (SA) by tuning the SPR frequency using Z-scan technique with 340 fs pulses at 515 nm. When combined with two-dimensional (2D) MoS_2, an enhanced SA response is observed for Ag/MoS_2 nanocomposites compared with the counterparts. The nonlinear absorption coefficient of Ag/MoS_2 nanocomposites is about $-(10.93 \pm 0.6) \times 10^{-2}$ cm·GW^{-1}, which is almost three times higher than that of MoS_2. Our work has an instructive value in promoting the potential application of AgNPs and its nanocomposites in optoelectronic and photonic devices, such as optical limiting and ultrafast laser pulse generation.

Keywords Silver nanoparticles · Two-dimensional molybdenum disulfide · Chemical synthesis · Nonlinear effects · Optical properties

✉ Xiao-Yan Zhang
xyzhang_dd@shu.edu.cn

✉ Yi Sun
sunyi082032@163.com

[1] Department of Chemistry, Shanghai University, Shanghai 200444, China

[2] Laboratory of Micro-Nano Photonic and Optoelectronic Materials and Devices, Key Laboratory of Materials for High-Power Laser, Shanghai Institute of Optics and Fine Mechanics (SIOM), Chinese Academy of Sciences (CAS), Shanghai 201800, China

[3] Center of Materials Science and Optoelectronic Engineering, University of Chinese Academy of Sciences, Beijing 100049, China

[4] Shanghai Aerospace Hydrogen Energy Technology Co., Ltd, Shanghai 201108, China

[5] State Key Laboratory of High Field Laser Physics, Shanghai Institute of Optics and Fine Mechanics (SIOM), Chinese Academy of Sciences (CAS), Shanghai 201800, China

1 Introduction

Metal nanoparticles (MNPs) with at least one dimension (length, width, or thickness) within a range of 1–100 nm, present exclusive physiochemical properties, such as high stability, exceptional optical properties and catalytic activities, enabling potential applications in catalysis [1], sensing [2, 3], energy storage [4], surface enhanced Raman scattering [5]. Among various MNPs, silver nanoparticles (AgNPs) were paid great attention to a variety of fields due to their unique physical and chemical properties, such as surface plasmon resonance (SPR) [6] and fluorescent properties [7], owing to their excellent photo-stability, good process ability, and extremely low toxicity. Generally, AgNPs with sizes of less than 2 nm, where the particle size is on the same order of the electron Fermi wavelength (0.5 nm), exhibit a fascinating fluorescent property, and become non-luminescent with the particle size approaching to the electron mean free path length (~ 50 nm), where collective excitations of electrons become dominant, leading to plasmon resonance [8, 9]. It has been reported that the SPR and fluorescent properties of silver nanostructures depend strongly on its

geometry and environment, such as the nanoparticle size [10] and shape [11]. Shang et al. [12] synthesized fluorescent Ag nanoclusters using the common and commercially available polyelectrolyte poly(methacrylic acid) as the template. The obtained Ag nanoclusters exhibit good photo-stability, pH- and excitation-dependent emission behavior, and a stimuli-responsive property, showing potential applications in a wide range such as bio-sensing. Luo et al. [13] obtained Ag nanorods with thin diameters and tunable aspect ratio using a seed-mediated approach. It is found that the transverse mode kept below 400 nm, while the longitudinal mode could be readily tuned from the visible to the near-infrared region by varying the aspect ratio. Tsuji et al. [14] studied the rapid sphere-to-prism (STP) transformation of AgNPs by monitoring the changing of SPR bands in the UV–Vis region. They reported that a key process for the STP transformation is shape-selective oxidative etching of spherical particles in a mixture of spheres and prisms with that the etching rate of spherical particles by H_2O_2 is faster than that of prisms. Scardaci et al. [15] found that the shape change of AgNPs from spherical to flat nanoparticles can tune the position of the main plasmon resonance across the visible and near-infrared part of the spectrum. Therefore, it is crucial for the controllable synthesis of AgNPs with desirable physicochemical properties.

Recently, the third-order nonlinear optical (NLO) properties of AgNPs and its nanocomposites have attracted a lot of attention due to its potential applications in optical switching [16] and ultrafast laser generation [17]. Gieseking et al. [18] found in theory that in linear silver nanowires, the longitudinal excited states show positive NLO polarizability which increases with nanowire length, while the transverse modes show a negative one. Wada et al. [19] fabricated a layered hybridized thin films composed of oriented polymers and AgNPs. They found that the existence of AgNPs in the hybrid thin films can significantly enhance the third-order NLO properties due to "excitation enhancement" induced by the localized SPR. Ferreira et al. [20] synthesized Au–Ag bimetallic nanoparticles and reported that the third-order NLO susceptibility can be tailored by modifying the thickness of shell. The NLO absorption of AgNPs contains a variety of processes like saturable absorption (SA), two-photon absorption (TPA), multiphoton absorption, excited state absorption (ESA), free-carrier absorption (FCA), and reverse saturable absorption (RSA), which have different applications in different areas. Generally, SA leads to decrease in absorption in the sample along with increase in the input intensity which can be used to generate ultrashort pulse lasers, whereas for TPA and other processes, the absorption in the sample increases along with increase in the input intensity resulting in optical limiting effect, which can be used for optical limiter to protect the electro-optical sensors and the eyes [21]. For example, Bhavitha et al. [22]

reported the optical limiting performance of Ag cluster and investigated the solvent effect at 532 nm using 5 ns laser pulse. Zvyagin et al. [23] observed optical limiting effect in AgNPs with spherical and triangular shapes using 10-ns laser pulses at 532 nm, respectively. It is found that the optical limiting effect was induced by the nonlinear light scattering. Maurya et al. [24] investigated the polymer effect on the nonlinear absorption of AgNPs using femtosecond (fs) laser pulses at 400 nm and found that the SA process can be suppressed at high concentration of the polymer. However, how to differentiate which process dominates the NLO performance remains challenging for AgNPs, especially for the optical limiting effect.

On the other hand, two-dimensional (2D) transition metal dichalcogenides (TMDs) show excellent NLO performances, such as giant TPA absorption in monolayer MoS_2 [25] and SA in few-layer MoS_2 [26, 27], with potential applications in ultrafast laser generation and optical limiting. Formation of hetero-structured nanocomposites of AgNPs and 2D TMDs is expected to further enhance the NLO absorption properties compared with their counterparts. Shao et al. [28] reported that introduction of AgNPs in WS_2-Ag nanocomposites can further enhance the nonlinear absorption of 2D WS_2 at nanosecond 532 nm. Poudel et al. [29] found a strong coupling of excitonic states in Ag-MoS_2 hybrids.

In this work, we used a simple chemical synthesis method to synthesize AgNP colloids using sodium citrate as stabilizing agent and sodium borohydride as reducing agent in water–ethanol solution by a simple mixing process. It is found that the addition of the amount of ethanol significantly affects the formation and growth of AgNPs in the colloids. The AgNP colloids synthesized with optical parameters can keep stable for several weeks without heating or stirring. Then, we investigated its linear and nonlinear optical properties by ultraviolet visible (UV–Vis) spectrophotometer and open-aperture Z-scan (Z is Z-axis, which is the optical axis) technique irradiated at 515 nm with 340 fs at a repetition rate of 1 kHz, respectively. A tunable nonlinear optical performance is observed by adjusting the SPR frequencies. In addition, the selectively synthesized AgNPs were found to be able to greatly enhance the NLO properties of 2D MoS_2 by forming hetero-structured nanocomposites.

2 Experimental

2.1 Synthesis of AgNPs colloids

All chemicals were analytical-grade reagents and used as received without further purification. Water used for this study was double-distilled water. Silver nitrate was used as precursor of silver to prepare AgNPs in colloidal solution

with a concentration of 0.8×10^{-4} mol·L^{-1} in the existence of sodium citrate as surfactant.

To investigate the effect of the ethanol on the morphology of the AgNPs and the stability of the colloids, a series of samples with different amounts of ethanol were prepared. Typically, 0.5 mL 5×10^{-3} mol·L^{-1} AgNO$_3$ was mixed with 30 mL of deionized water and 0.1 mL 1 wt% sodium citrate, followed by addition of 0.1 mL 1 mg·mL^{-1} sodium borohydride gradually without stirring at room temperature. The color of the mixture turned slowly from colorless to yellow. The obtained sample was denoted as AgNPs(0), where 0 means 0 mL ethanol. By increasing the amount of ethanol from 0 to 15, 20, and 25 mL, a series of AgNPs aqueous colloids were obtained, denoted as AgNPs(15), AgNPs(20), AgNPs(25), respectively.

2.2 Synthesis of AgNPs/MoS$_2$ nanocomposites

The AgNPs/MoS$_2$ nanocomposites were synthesized via a simple two-step process. First, it is the synthesis of 2D MoS$_2$ by liquid-exfoliated method [26]. Typically, MoS$_2$ powders (5 mg·mL^{-1}) were dispersed in 90% ethanol aqueous solution and ultra-sonicated in a water bath for 24 h without addition of any other surfactants. The dispersions after standing for 24 h were centrifuged at 3000 r·min^{-1} for 90 min to remove the un-exfoliated powders. The top two-thirds of the dispersions were collected for use. Then, similar to the synthesis of AgNPs(25) colloids, Ag/MoS$_2$ hetero-structured nanocomposites were in situ synthesized in 2D MoS$_2$ solutions by adding sequentially Ag precursors, sodium citrate and NaBH$_4$ with the volume of ethanol as 25 mL.

2.3 Characterizations

UV–Vis absorption spectra were measured for the samples with a PerkinElmer Lambda 750 instrument in the range of 250–800 nm. Transmission electron microscopy (TEM) and high-resolution TEM (HRTEM) were carried out with a JEOL 3010 instrument. The samples were drop-cast on carbon-coated copper grids (400 meshes) and allowed to dry under ambient conditions.

2.4 NLO measurements

An open-aperture Z-scan system was used to investigate the third-order NLO properties of AgNPs and AgNPs/MoS$_2$ aqueous solution in a quartz cuvette with a thickness of 1 mm using a mode-locked fiber laser operating at 515 nm with 340 fs pulses at a 1 kHz repetition rate [30]. Total transmittance through the samples as a function of incident intensity was measured while the samples were gradually moved through the focus of a lens along the Z-axis. The beam waist

radii of the focus at 515 nm were estimated to be ~ 30 μm. In our experiments, the excitation power is limited in a range within which Z-scan curves are readily reproducible without any change in linear transmittance to avoid laser damage.

3 Results and discussion

3.1 Characterization of the fabricated AgNPs colloids

A series of AgNP colloids was synthesized with different amounts of ethanol. Figure 1 shows the UV–Vis absorption spectra of the series of AgNP colloids with the detailed synthesis parameters shown in Table 1. Obviously, samples AgNPs(0), AgNPs(15) and AgNPs(20) exhibit only one SPR peak at ~ 400 nm [31], while AgNPs(25) revealed two SPR bands with the color of the solution displaying light purple (Fig. 1a, c). According to previous reports, the one at ~ 400 nm is ascribed to the transverse plasmon mode, and the other one at ~ 520 nm is ascribed to the longitudinal mode, demonstrating a non-spherical morphology of AgNPs in AgNPs(25) [13, 32]. Gao et al. [33] also reported the SPR bands evolution along with the shape of AgNPs changing from isotropic sphere to anisotropic triangle from only one mode at ~ 450 nm to two modes with another at ~ 600–800 nm. On the other hand, the symmetry of the SPR peak at ~ 400 nm becomes poorer along with increasing the amount of ethanol, suggesting the shape of the AgNPs grows gradually non-spherical [33, 34]. The results demonstrate the addition of ethanol plays a vital role on controlling the shape of AgNPs. By increasing the volume ratio of ethanol in the system to a suitable value, two SPR modes will be observed for the obtained AgNPs colloids.

By comparing the positions of the SPR peak at ~ 400 nm for the samples (Fig. 1a), a little red-shift from ~ 401 to ~ 403 nm then to ~ 416 nm occurs along with increasing the volume of ethanol (V_E) from 0 to 15 mL, and then to 20 mL. The red-shift is probably ascribed to the increased anisotropy with higher aspect ratio of the AgNPs induced by the increase of the ethanol amount [11, 35], which is further proved by the following TEM results. The refraction index of the host media may also contribute to the red-shift with the refraction index increasing from ~ 1.33 for AgNPs(0) to about 1.36 for AgNPs(25) [36].

To monitor the colloidal stability of the samples in a quantitative manner, we measured the absorption intensity at 407 nm per unit cell length (*l*). Figure 1b shows Absorption$_{407}$ (A_{407})/*l* as a function of time for dispersions for AgNPs(0), AgNPs(15), AgNPs(20) and AgNPs(25), respectively. Obviously, sample AgNPs(15) reveals the highest dispersion ability. This is due to that the increasing amount of ethanol can accelerate the reduction rate of
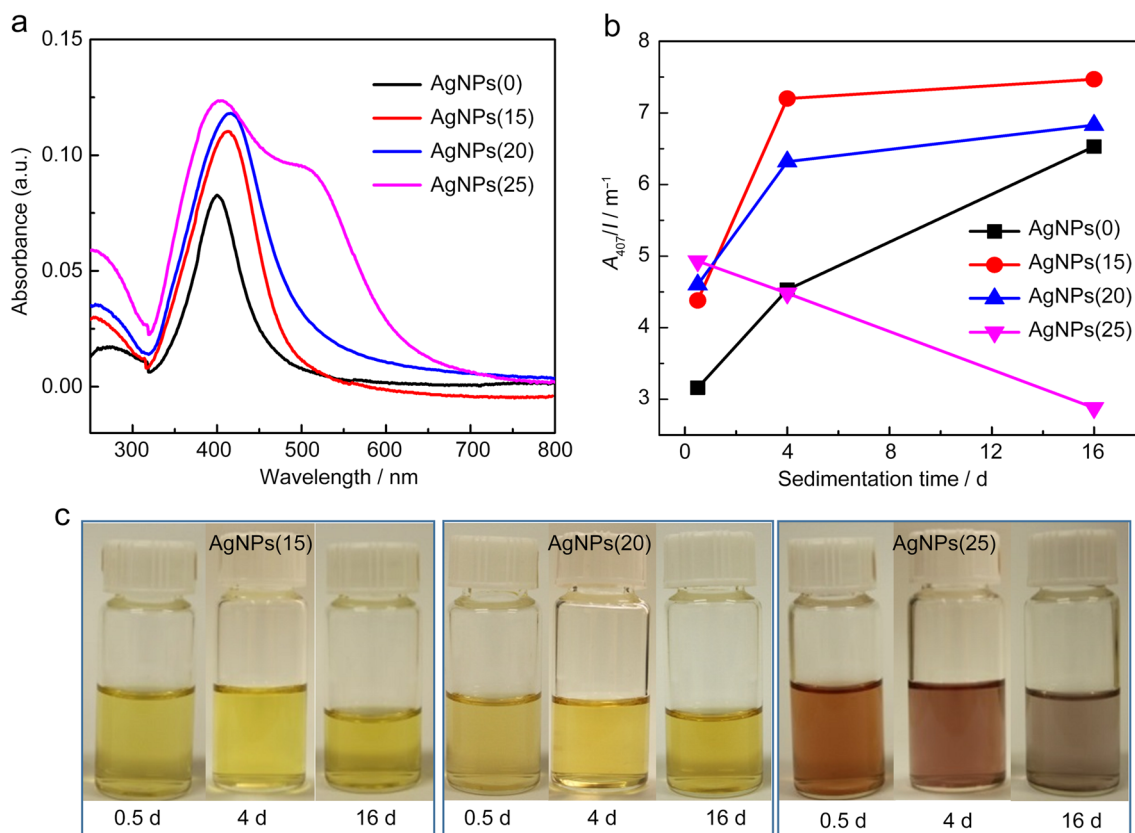
Fig. 1 Effect of ethanol on the absorption for the prepared AgNPs colloidal solution. **a** Linear absorption spectra for the Ag colloidal solution prepared with the amount of ethanol as 0, 15, 20 and 25 mL, respectively. **b** A_{407}/l versus sedimentation time for the obtained AgNPs colloid solution. **c** Photographs of the colloids with different storage times. Note: d means days

Table 1 Synthesis parameters for the AgNP colloids

Sample	$C_A/(mol \cdot L^{-1})$	V_S/mL	V_B/mL	V_W/mL	V_E/mL	Phenomenon
AgNPs(0)	0.8×10^{-4}	0.1	0.1	30	0	Yellow
AgNPs(15)	0.8×10^{-4}	0.1	0.1	15	15	Yellow
AgNPs(20)	0.8×10^{-4}	0.1	0.1	10	20	Yellow
AgNPs(25)	0.8×10^{-4}	0.1	0.1	5	25	Purple

Note: C_A is the concentration of $AgNO_3$; V_S is the volume of 1% sodium citrate; V_B is the volume of 1 mg·mL^{-1} $NaBH_4$; V_W is the volume of deionized water; V_E is the volume of absolute ethanol

$AgNO_3$, which results in the highest stability of AgNPs(15) with moderate reaction rate among the series of samples. As demonstrated by Morales-Bonilla et al. [37], the NPs with sizes smaller than 17 nm will stay suspended in the solution with a good stability, which is in consistent with our results. Combined with the following TEM results, the poor dispersion ability of sample AgNPs(25) can be ascribed to the larger sizes of un-spherical AgNPs with obvious larger aspect ratio compared with the other three samples.

The morphology of the prepared AgNPs in the colloidal solution was characterized by TEM and HRTEM. Figure 2a–c reveals the typical TEM images of the samples synthesized with different amounts of ethanol. The AgNPs show an average diameter of ~ 15 nm and well crystal structure with the average size slightly increasing with increasing the amount of ethanol. Clearly, the AgNPs in AgNPs(0) and AgNPs(15) present spherical morphology. While for AgNPs(25), the AgNP displays an obvious elliptical morphology (Fig. 2c), leading to the appearance of the longitudinal mode at ~ 520 nm. The results are consistent with the results of the UV–Vis absorption spectra. The lattice spacing of 0.23 nm was observed from the HRTEM image in Fig. 2d, which is corresponding to the {111} planes of Ag [13].
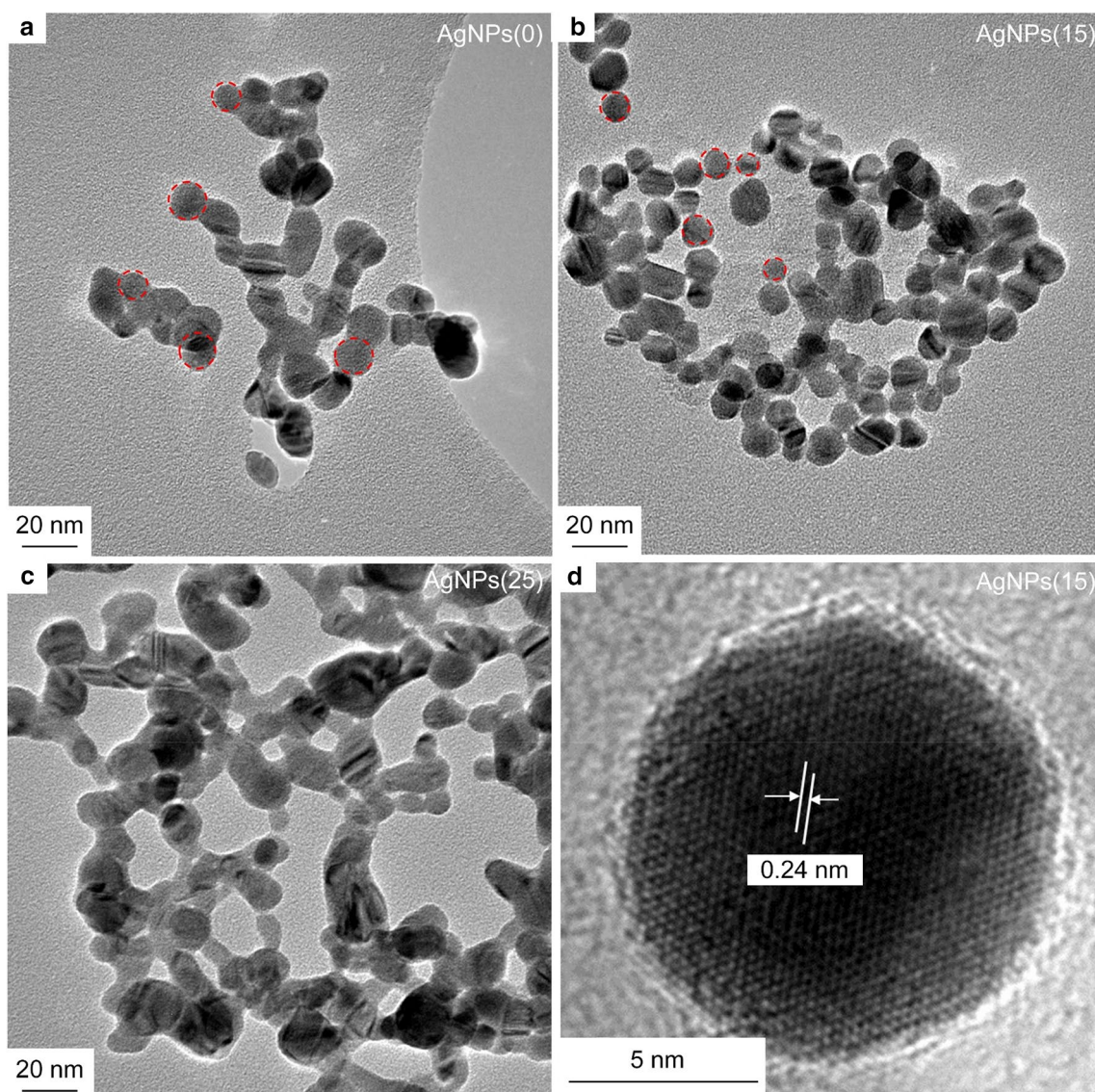
Fig. 2 Typical TEM images of **a–c** AgNPs(0), AgNPs(15) and AgNPs(25). **d** Typical HRTEM image of a AgNP for sample AgNPs(15)

3.2 NLO performances of the AgNPs colloids

Based on the above results, we chose samples AgNPs(15) and AgNPs(25) as the typical samples to investigate their NLO properties and the dominant mechanism using Z-scan setup. The open-aperture Z-scan system was illustrated in Fig. 3. This experimental set-up has been successfully used in measuring the NLO performances of graphene and 2D TMDs [38, 39].

Figure 4 shows the typical Z-scan curves of AgNPs(15) and AgNPs(25) excited by 515 nm (340 fs). As shown in Fig. 4a, the AgNPs(15) colloids exhibit obvious optical limiting response, while sample AgNPs(25) shows obvious SA response (Fig. 4b). In our case, the thermal effects can be neglected because the samples were excited by femtosecond
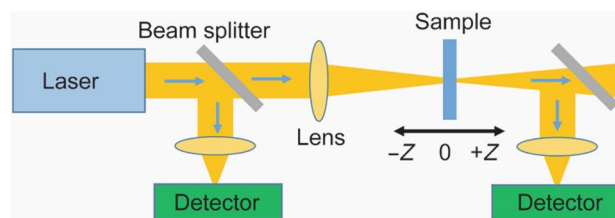

Fig. 3 Schematic of the adopted open-aperture Z-scan set-up

laser pulses with low irradiance intensity which have weak peak intensity [40]. So, the observed optical limiting response can be attributed to the absorption, such as TPA, multi-photon absorption, ESA, FCA, or RSA. For FCA effect, the critical fluence is:
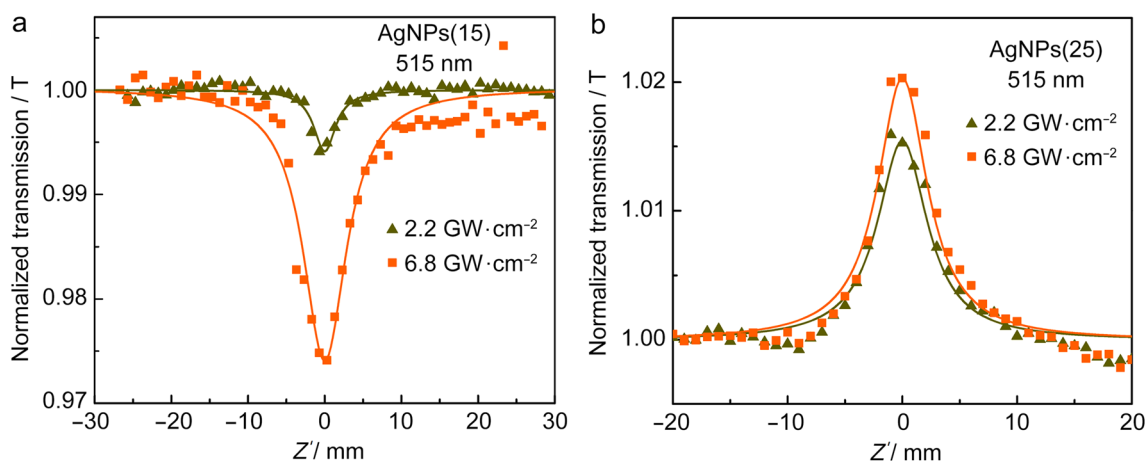
Fig. 4 Typical Z-scan results for the samples **a** AgNPs(15) and **b** AgNPs(25) under excitation of femtosecond laser at 515 nm with a pulse width of 340 fs. The solid symbols denote the experimental data and the solid lines represent the theoretical fits, and Z' represents the distance from sample to focus

$$F_C = 4\sqrt{2}\hbar\omega[\sigma(1 - R)], \tag{1}$$

where σ is the FCA absorption cross section and R is the surface reflectivity which is much higher when compared with the onset fluence for TPA. The estimated F_C in previous report is ~ 0.1 J·cm^{-2}, which is approximately two orders of magnitude larger than the fluence in our experiment [41]. This means the FCA effect can also be neglected. At the same time, AgNPs(15) shows only one SPR peak at ~ 400 nm (~ 3.1 eV) with the photon energy larger than that of the excitation laser (515 nm, 2.4 eV) which needs to absorb two photons to excite the surface plasmons. For AgNPs(25), two SPR modes were observed with one at ~ 400 nm and the other at ~ 520 nm with the photon energy smaller than that of the excitation laser, making it possible to absorb one photon to excite the surface plasmons. This means that only TPA exists in AgNPs(15), while TPA and SA co-exist in AgNPs(25). Considering that the irradiation wavelength of 515 nm is near to the longitudinal SPR mode at ~ 520 nm, it is reasonable to assume that SA is dominant in AgNPs(25) [42]. This explains why AgNPs(15) exhibits TPA response while AgNPs(25) shows SA response.

To quantitatively determine the NLO characteristics of AgNP colloids, the Z-scan data were fitted using the propagation equation in the form of Eq. (2) [43, 44],

$$\frac{dI(z')}{dz'} = -\alpha_0 I(z') - \beta_{eff} I^2(z'), \tag{2}$$

where $I(z')$ is the laser beam intensity through the sample, z' is the propagation depth in the sample, α_0 is the linear absorption coefficient of the sample, and β_{eff} is the nonlinear absorption coefficient. In the case of SA, β_{eff} is negative, while in the case of TPA, β_{eff} is positive. This Eq. (2) can be

solved exactly, and the normalized power transmission $T(z)$ is seen in Ref. [38]

$$T(z) = \left[\ln\left(1 + \beta_{eff}I_0 L_{eff}\left(1 + z^2/z_0^2\right)\right)\right]/\left[\beta_{eff}I_0 L_{eff}\left(1 + z^2/z_0^2\right)\right], \tag{3}$$

where $L_{eff} = (1 - e^{-\alpha_0 L})/\alpha_0$ is the sample's effective thickness, which is the optical length of the adopted cuvettes (1 mm), I_0 is the on-axis irradiance at the focus, L is the sample's real thickness, and z_0 is the beam's diffraction length.

The solid lines in Fig. 4a and b are the fitting curves based on the nonlinear absorption model and agree well with the experimental data. The fitting parameters are shown in Table 2. The nonlinear absorption coefficient β_{eff} was fitted to be $(1.96 \pm 0.4) \times 10^{-2}$ cm·GW^{-1} and $-(7.90 \pm 0.4) \times 10^{-2}$ cm·GW^{-1} at the irradiance intensity of $\sim (2.2 \pm 1.2)$ GW·cm^{-2} for AgNPs(15) and AgNPs(25), respectively. The TPA coefficient β_{eff} for AgNPs(15) is increased to $(5.81 \pm 0.4) \times 10^{-2}$ cm·GW^{-1}, while the SA coefficient β_{eff} for AgNPs(25) kindly decreased to $-(3.45 \pm 0.6) \times 10^{-2}$ cm·GW^{-1} with increased irradiance intensity to (6.8 ± 1.2) GW·cm^{-2}, respectively. The irradiance-dependent TPA coefficient was reported previously by Zhang et al. [38]. The deviation of the nonlinearity at different irradiances for AgNPs(25) can be mainly due to the experimental errors (Table 2). The strong SA absorption response of AgNPs(25) can be ascribed to the relatively strong longitudinal resonant absorption (~ 520 nm) near the excitation wavelength at 515 nm, resulting in prominent SA response induced by one-photon absorption [45]. López-Suárez et al. [46] observed the variation of TPA to SA in AgNPs with only one SPR band at ~ 400 nm under off-resonance excitation, which is caused by the small difference in the magnitude of the absorbance values and SPR peak positions. In our work, the two AgNPs samples exhibit significantly different linear

Table 2 Linear and NLO parameters of the AgNP colloid excited at 515 nm in the fs region

Sample	Irradiance (GW·cm^{-2})	T (%)	α_0 (cm)	I_{sat} (GW·cm^{-2})	β_{eff} (cm·GW^{-1}, $\times 10^{-2}$)	Im $\chi^{(3)}$ (esu, $\times 10^{-14}$)	FOM (esu·cm^{-1}, $\times 10^{-14}$)
AgNPs(15)	2.2 ± 1.2	89.5	1.11	–	1.96 ± 0.4	0.64 ± 0.01	0.57 ± 0.01
	6.8 ± 1.2	89.5	1.11	–	5.81 ± 0.4	1.88 ± 0.01	1.70 ± 0.01
AgNPs(25)	2.2 ± 1.2	85.5	1.57	17.72	$-(7.90 \pm 0.4)$	$-(2.56 \pm 0.13)$	1.63 ± 0.09
	6.8 ± 1.2	85.5	1.57	39.42	$-(3.45 \pm 0.6)$	$-(1.12 \pm 0.19)$	0.71 ± 0.02
MoS$_2$	26.4 ± 1.5	73.9	3.03	25.38	$-(3.71 \pm 0.6)$	$-(1.20 \pm 0.19)$	0.40 ± 0.01
Ag/MoS$_2$	26.4 ± 1.5	67.4	3.95	16.57	$-(10.93 \pm 0.6)$	$-(3.54 \pm 0.19)$	0.90 ± 0.03

absorption in the UV–Vis region as shown in Fig. 1. Thus, in our experimental conditions, only TPA occurs for the sample with only one SPR band, while both TPA and SA co-exist in the sample with two SPR bands with SA dominant due to the on-resonance irradiation. This phenomenon reveals that the on/off resonance of SA/TPA near the SPR frequency plays an important role in adjusting the NLO response [44]. The imaginary third-order susceptibility Im$\chi^{(3)}$ can be approximately expressed in Eq. (4):

$$\text{Im}\chi^{(3)} = \left[\left(10^{-7} c \lambda n^2 \right) / \left(96 \pi^2 \right) \right] \beta_{eff}, \tag{4}$$

where c, λ, and n are the light speed in vacuum, wavelength of the laser pulses, and the refractive index, respectively. Here, n is taken as 1.36. The figure of merit (FOM) for the third-order optical nonlinearity is defined as:

$$\text{FOM} = \left| \text{Im}\chi^{(3)} / \alpha_0 \right|. \tag{5}$$

The calculated Im$\chi^{(3)}$ and FOM for the two typical samples are shown in Table 2.

To further study the SA characteristic of the AgNPs colloids, we fitted the Z-scan data using the following equation:

$$T(z) = \left[1 - \frac{I_{sat} \times \Delta R}{I_{sat} + I_0 / \left(1 + Z^2 / Z_0^2 \right)} \right] \Big/ (1 - \Delta R), \tag{6}$$

where ΔR and I_{sat} are the modulation depth and saturation intensity, respectively. As shown in Fig. 4b, the modulation depth is 2.1%. By fitting the curve, the saturation intensity of the AgNPs colloids was calculated to be 39.42 GW·cm^{-2} at irradiance of (6.8 ± 1.2) GW·cm^{-2}. As shown in Table 2, the saturation intensity I_{sat} becomes larger at higher irradiance, which can be explained by a weak saturation effect [44]. Additionally, both the relative absorption intensity and the position of the longitudinal SPR band are dependent on the aspect ratio of the anisotropic AgNPs [13]. The NLO absorption in the anisotropic nanoparticle can be greatly influenced by its aspect ratio. Our work demonstrates that the varied NLO performances from SA to TPA can be realized for AgNPs by adjusting its SPR frequencies, which is

meaningful in practical applications. Gorham et al. [47] reported that if AgNPs is oxidized, the SPR bands will disappear with obvious color loss. In our work, no color loss is observed for the AgNPs colloids during measuring process with the Z-scan results repeatable, suggesting that no oxidation of AgNPs occurs under the experimental conditions.

3.3 NLO properties of AgNPs/MoS$_2$ nanocomposites

It has been reported that 2D MoS$_2$ shows SA response under the excitation of femtosecond laser pulses in a wide range from visible light region to near-infrared region [25, 48]. Thus, we choose AgNPs(25) with SA behavior to form composites with 2D MoS$_2$. Figure 5a shows the linear absorption spectra of MoS$_2$ and Ag/MoS$_2$ nanocomposites. The characteristic bands at 623 and 670 nm corresponding to few-layered MoS$_2$ are observed for both two samples, which are ascribed to the A and B excitonic transitions arising from the K point of the Brillouin zone [49]. Compared with pure MoS$_2$ dispersions, the nanocomposites exhibit higher absorption in the UV–Vis range, which is due to the surface plasmon band of AgNPs as shown by the arrows.

Their NLO properties were investigated using Z-scan technique under the same conditions with those of AgNPs. Figure 5b shows the typical Z-scan curves of MoS$_2$ and Ag/MoS$_2$ suspensions. As expected, the nanocomposites show enhanced SA response compared with that of pure MoS$_2$ under the same measuring conditions. By fitting the experimental data, the nonlinear absorption coefficient β_{eff} was obtained to be $-(3.71 \pm 0.6) \times 10^{-2}$ cm·GW^{-1} and $-(10.93 \pm 0.6) \times 10^{-2}$ cm·GW^{-1} at the irradiance intensity of (26.4 ± 1.5) GW·cm^{-2} for MoS$_2$ and Ag/MoS$_2$ suspensions (Table 2), respectively. The β_{eff} for Ag/MoS$_2$ nanocomposites was almost three times that of MoS$_2$ suspensions, and two times that of AgNPs(25) with an average SA coefficient of $-(3.71 \pm 0.6) \times 10^{-2}$ cm·GW^{-1}. Combined with previous reports, the NLO enhancement compared with single components can be ascribed to the SPR of AgNPs and the charge transfer between AgNPs and MoS$_2$ [50].
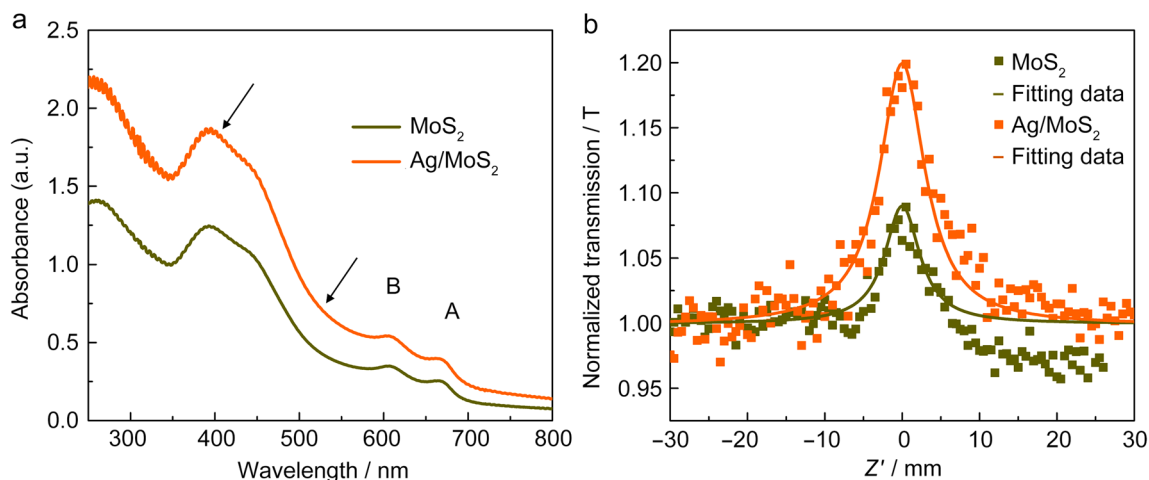
Fig. 5 **a** Linear absorption spectra and **b** typical Z-scan results for the samples MoS_2 and Ag/MoS_2 suspensions under excitation of femtosecond laser at 515 nm with a pulse width of 340 fs. The solid symbols denote the experimental data and the solid lines represent the theoretical fits

4 Conclusion

In summary, we investigated the NLO performances of the fabricated AgNP colloids and realized the tunable NLO performances from TPA to SA. The linear optical spectra results demonstrate that only a typical SPR band is observed at ~400 nm for AgNPs(0) and AgNPs(15) colloids with low ethanol amount. When increasing the ethanol amount, another longitudinal SPR mode occurs for sample AgNPs(25) at ~520 nm. For the ultrafast NLO investigation, the optical limiting effect for sample AgNPs(15) was switched into SA effect for sample AgNPs(25). The controllability can be attributed to their different SPR frequencies which induce dominant TPA occurrence for AgNPs(15) and SA for AgNPs(25). The prominent SA behavior is caused by the strong longitudinal resonant absorption near the excitation wavelength at 515 nm. Additionally, we controllably synthesized nanocomposites of Ag/MoS_2 utilizing the resonant absorption near the excitation wavelength at 515 nm, which exhibited enhanced NLO property, almost three times that of MoS_2 suspensions. The present results are beneficial to in-depth understanding of the ultrafast NLO absorption properties of AgNPs and to promote the practical applications of AgNPs and its nanocomposites in different fields.

Author contributions Xiao-Yan Zhang and Wei Zhou wrote the draft; Xiao-Yan Zhang and Hong-Qiang Wang collected the data; Yi Sun and Jun Wang contributed to conceived the idea of the study. All authors contributed to the writing and revisions.

Declarations

Conflict of interest The authors declare no conflict of interest.

References

1. Vadakkekara R, Chakraborty M, Parikh PA. Catalytic performance of silica-supported silver nanoparticles for liquid-phase oxidation of ethylbenzene. Ind Eng Chem Res. 2012;51:5691.
2. Fereja SL, Li P, Guo JH, Fang ZY, Zhang ZW, Zhuang ZH, Zhang XH, Liu KF, Chen W. Silver-enhanced fluorescence of bimetallic Au/Ag nanoclusters as ultrasensitive sensing probe for the detection of folic acid. Talanta. 2021;233:122469.
3. Fredj Z, Ben Ali M, Abbas MN, Dempsey E. Simultaneous determination of ascorbic acid, uric acid and dopamine using silver nanoparticles and copper monoamino-phthalocyanine functionalised acrylate polymer. Anal Methods. 2020;12(31):3883.
4. Ramirez N, Zambo D, Sardella F, Kissling PA, Schlosser A, Graf RT, Pluta D, Deiana C, Bigall NC. Pd-doped cellulose carbon aerogels for energy storage applications. Adv Mater Interfaces. 2021;8:2100310.
5. Xu K, Zhou R, Takei K, Hon M. Toward flexible surface enhanced Raman scattering (SERS) sensors for point-of-care diagnostics. Adv Sci. 2019;6:1900925.
6. Liu LT, Aleisa R, Zhang Y, Feng J, Zheng YQ, Yin YD, Wang WS. Dynamic color-switching of plasmonic nanoparticle films. Angew Chem Int Ed. 2019;58(45):16307.
7. Peyser LA, Vinson AE, Bartko AP, Dickson RM. Photoactivated fluorescence from individual silver nanoclusters. Science. 2001;291:103.
8. Zheng J, Ding Y, Tian BZ, Wang ZL, Zhuang XW. Luminescent and Raman active silver nanoparticles with polycrystalline structure. J Am Chem Soc. 2008;130:10472.
9. Aikens CM, Li SZ, Schatz GC. From discrete electronic states to plasmons: TDDFT optical absorption properties of Ag-n (n

= 10, 20, 35, 56, 84, 120) tetrahedral clusters. J Phys Chem C. 2008;112:11272.

10. Roy S, Baral A, Banerjee A. Tuning of silver cluster emission from blue to red using a bio-active peptide in water. ACS Appl Mater Interfaces. 2014;6:4050.

11. Cieśla J, Chylińska M, Zdunek A, Szymańska-Chargot M. Effect of different conditions of synthesis on properties of silver nanoparticles stabilized by nanocellulose from carrot pomace. Carbohydr Polym. 2020;245:116513.

12. Shang L, Dong SJ. Facile preparation of water-soluble fluorescent silver nanoclusters using a polyelectrolyte template. Chem Commun. 2008;44(9):1088.

13. Luo M, Huang H, Choi SI, Zhang C, da Silva RR, Peng HC, Li ZY, Liu J, He Z, Xia Y. Facile synthesis of Ag nanorods with no plasmon resonance peak in the visible region by using Pd decahedra of 16 nm in size as seeds. ACS Nano. 2015;9:10523.

14. Tsuji M, Gomi S, Maeda Y, Matsunaga M, Hikino S, Uto K, Tsuji T, Kawazumi H. Rapid transformation from spherical nanoparticles, nanorods, cubes, or bipyramids to triangular prisms of silver with PVP, citrate, and H_2O_2. Langmuir. 2012;28:8845.

15. Scardaci V, Pulvirenti M, Condorelli M, Compagnini G. Monochromatic light driven synthesis and growth of flat silver nanoparticles and their plasmon sensitivity. J Mater Chem C. 2020;8:9734.

16. Haghighatzadeh A. Enhanced third-order optical susceptibility in Ag-doped CeO_2 nanostructures under pulsed Nd-YVO_4 laser. Opt Laser Technol. 2020;126:106114.

17. Liu WJ, Liu ML, Lin S, Liu JC, Lei M, Wu H, Dai CQ, Wei ZY. Synthesis of high quality silver nanowires and their applications in ultrafast photonics. Opt Express. 2019;27(12):16440.

18. Gieseking RLM. Third-order nonlinear optical properties of Ag nanoclusters: connecting molecule-like and nanoparticle-like behavior. Chem Mater. 2019;31:6850.

19. Wada K, Onodera T, Kasai H, Sato R, Takeda Y, Oikawa H. Third-order nonlinear optical properties of layered type hybridized thin films consisting of oriented polydiacetylene nanofibers and silver nanoparticles. J Phys Chem C. 2019;123:25781.

20. Ferreira E, Kharisov B, Vázquez A, Méndez EA, Severiano-Carrillo I, Trejo-Durán M. Tuning the nonlinear optical properties of Au@Ag bimetallic nanoparticles. J Mol Liq. 2020;298:112057.

21. Zhu JH, Li YX, Chen Y, Wang J, Zhang B, Zhang JJ, Blau WJ. Graphene oxide covalently functionalized with zinc phthalocyanine for broadband optical limiting. Carbon. 2011;49:1900.

22. Bhavitha KB, Nair AK, Perumbilavil S, Joseph S, Kala MS, Saha A, Narayanan RA, Hameed N, Thomas S, Oluwafemi OS. Investigating solvent effects on aggregation behaviour, linear and nonlinear optical properties of silver nanoclusters. Opt Mater. 2017;73:695.

23. Zvyagin AI, Perepelitsa AS, Lavlinskaya MS, Ovchinnikov OV, Smirnov MS, Ganeev RA. Demonstration of variation of the nonlinear optical absorption of nonspherical silver nanoparticles. Optik. 2018;175:93.

24. Maurya SK, Ganeev RA, Rout A, Guo C. Influence of PVP polymer concentration on nonlinear absorption in silver nanoparticles at resonant excitation. Appl Phys A. 2020;126:26.

25. Li YX, Dong NN, Zhang SF, Zhang XY, Feng YY, Wang KP, Zhang L, Wang J. Giant two-photon absorption in monolayer MoS_2. Laser Photonics Rev. 2015;9(4):427.

26. Zhang XY, Zhang SF, Chang CX, Feng YY, Li YX, Dong NN, Wang KP, Zhang L, Blau WJ, Wang J. Facile fabrication of wafer-scale MoS_2 neat films with enhanced third-order nonlinear optical performance. Nanoscale. 2015;7(7):2978.

27. Zhang XY, Zhang SF, Xie YF, Huang JW, Wang L, Cui Y, Wang J. Tailoring the nonlinear optical performance of two-dimensional MoS_2 nanofilms via defect engineering. Nanoscale. 2018;10:17924.

28. Shao YB, Chen C, Han J, Kong D, Wu WZ, Gao YC. Enhanced nonlinear optical absorption of WS_2 by Ag nanoparticles. Ferroelectrics. 2020;563:177.

29. Poudel Y, Lim GN, Moazzezi M, Hennighausen Z, Rostovtsev Y, D'Souza F, Kar S, Neogi A. Active control of coherent dynamics in hybrid plasmonic MoS_2 monolayers with dressed phonons. ACS Photonics. 2019;6:1645.

30. Wang J, Hernandez Y, Lotya M, Coleman JN, Blau WJ. Broadband nonlinear optical response of graphene dispersions. Adv Mater. 2009;21:2430.

31. Wiley B, Im S, Li Z, McLellan JM, Siekkinen A, Xia Y. Maneuvering the surface plasmon resonance of silver nanostructures through shape-controlled synthesis. J Phys Chem B. 2006;110:15666.

32. Zook JM, Long SE, Cleveland D, Geronimo CLA, MacCuspie RI. Measuring silver nanoparticle dissolution in complex biological and environmental matrices using UV–Visible absorbance. Anal Bioanal Chem. 2011;401:1993.

33. Gao MJ, Sun L, Wang ZQ, Zhao YB. Controlled synthesis of Ag nanoparticles with different morphologies and their antibacterial properties. Mater Sci Eng C. 2013;33:397.

34. Fernandez-Hernandez RC, Gleason-Villagran R, Torres-Torres C, Rodriguez-Fernandez L, Crespo-Sosa A, Cheang-Wong JC, Lopez-Suarez A, Rangel-Rojo R, Oliver A, Reyes-Esqueda JA. On the physical contributions to the third-order nonlinear optical response in plasmonic nanocomposites. J Opt. 2012;14:125203.

35. Campos A, Troc N, Cottancin E, Pellarin M, Weissker HC, Lermé J, Kociak M, Hillenkamp M. Plasmonic quantum size effects in silver nanoparticles are dominated by interfaces and local environments. Nat Phys. 2019;15:275.

36. Noguez C. Surface plasmons on metal nanoparticles: the influence of shape and physical environment. J Phys Chem C. 2007;111:3806.

37. Morales-Bonilla S, Torres-Torresa C, Trejo-Valdez M, Torres-Torres D, Urriolagoitia-Calderóna G. Mechano-optical transmittance and third order nonlinear optical properties exhibited by Au nanoparticles. Optik. 2015;126:4093.

38. Zhang SF, Dong NN, McEvoy N, O'Brien M, Winters S, Berner NC, Yim CY, Li YX, Zhang XY, Chen ZH, Zhang L, Duesberg GS, Wang J. Direct observation of degenerate two-photon absorption and its saturation in WS_2 and MoS_2 monolayer and few-layer films. ACS Nano. 2015;9:7142.

39. Cheng X, Dong NN, Li B, Zhang XY, Zhang SF, Jiao J, Blau WJ, Zhang L, Wang J. Controllable broadband nonlinear optical response of graphene dispersions by tuning vacuum pressure. Opt Express. 2013;21(14):16486.

40. Allu R, Banerjee D, Avasarala R, Hamad S, Rao SV, Podagatlapalli GK. Broadband femtosecond nonlinear optical properties of silver nanowire films. Opt Mater. 2019;96:109305.

41. Boggess TF, Bohnert KM, Mansour K, Moss SC, Boyd IW, Smirl AL. Simultaneous measurement of the two-photon coefficient and free-carrier cross section above the bandgap of crystalline silicon. IEEE J Quantum Electron. 1986;22:360.

42. Torres-Torres C, Tamayo-Rivera L, Rangel-Rojo R, Torres-Martínez R, Silva-Pereyra HG, Reyes-Esqueda JA, Rodríguez-Fernández L, Crespo-Sosa A, Cheang-Wong JC, Oliver A. Ultrafast optical phase modulation with metallic nanoparticles in ion-implanted bilayer silica. Nanotechnology. 2011;22:355710.

43. Sheik-Bahae M, Said AA, Wei TH, Hagan DJ, Van Stryland EW. Sensitive measurement of optical nonlinearities using a single beam. IEEE J Quantum Electron. 1990;26:760.

44. Zhang SF, Li YX, Zhang XY, Dong NN, Wang KP, Hanlon D, Coleman JN, Zhang L, Wang J. Slow and fast absorption saturation of black phosphorus: experiment and modelling. Nanoscale. 2016;8:17374.

45. Hari M, Mathew S, Nithyaja B, Joseph SA, Nampoori VPN, Radhakrishnan P. Saturable and reverse saturable absorption in aqueous silver nanoparticles at off-resonant wavelength. Opt Quantum Electron. 2012;43:49.

46. López-Suárez A, Torres-Torres C, Can-Uc B, Rangel-Rojo R, Valencia CE, Oliver A. Third-order nonlinear optical properties exhibited by a bilayer configuration of silver nanoparticles integrated to silicon nanocrystals embedded in ion-implanted silica. J Opt Soc Am B. 2015;32(5):805.

47. Gorham JM, MacCuspie RI, Klein KL, Fairbrother DH, Holbrook RD. UV-induced photochemical transformations of citrate-capped silver nanoparticle suspensions. J Nanopart Res. 2012;14:1139.

48. Wang KP, Wang J, Fan JT, Lotya M, O'Neill A, Fox D, Feng YY, Zhang XY, Jiang BX, Zhao QZ, Zhang HZ, Coleman JN, Zhang L, Blau WJ. Ultrafast saturable absorption of two-dimensional MoS$_2$ nanosheets. ACS Nano. 2013;7(10):9260.

49. Coleman JN, Lotya M, O'Neill A, Bergin SD, King PJ, Khan U, Young K, Gaucher A, De S, Smith RJ, Shvets IV, Arora SK, Stanton G, Kim HY, Lee K, Kim GT, Duesberg GS, Hallam T, Boland JJ, Wang JJ, Donegan JF, Grunlan JC, Moriarty G, Shmeliov A, Nicholls RJ, Perkins JM, Grieveson EM, Theuwissen K, McComb DW, Nellist PD, Nicolosi V. Two-dimensional nanosheets produced by liquid exfoliation of layered materials. Science. 2011;331:568.

50. Ebrahimzadeh M, Haghighatzadeh A, Dutta J. Improved third-order optical nonlinearities in Ag/MoS$_2$ Schottky-type nano/hetero-junctions. Opt Laser Technol. 2021;140:107092.

Dr. Xiao-Yan Zhang is currently vice professor at Department of Chemistry of the Shanghai University, China. She received her Ph.D. degree from the Fudan University in 2012. Before joining Shanghai University, she worked at Shanghai Institute of Optics and Fine Mechanics, Chinese Academy of Sciences for over 7 years. Dr. Zhang's research focuses on the synthesis, characterization and application of metal/semiconductor or nanomaterials for use in renewable energy conversion system.